IOP Conf. Series: Journal of Physics: Conf. Series **847** (2017) 012057 doi:10.1088/1742-6596/847/1/012057

Using 3D dosimetry to quantify the Electron Return Effect (ERE) for MR-image-guided radiation therapy (MR-IGRT) applications

Hannah J Lee[1,2], Gye Won Choi[1,2], Mamdooh Alqathami[1], Mo Kadbi[3], Geoffrey Ibbott[1]
[1]Department of Radiation Physics, UT MD Anderson Cancer Center, Houston, TX
[2]UT at Houston Graduate School of Biomedical Sciences, Houston, TX
[3]MR Therapy, Philips healthTech, Cleveland, OH

E-mail: gibbott@mdanderson.org

Abstract. Image-guided radiation therapy (IGRT) using computed tomography (CT), cone-beam CT, MV on-board imager (OBI), and kV OBI systems have allowed for more accurate patient positioning prior to each treatment fraction. While these imaging modalities provide excellent bony anatomy image quality, MRI surpasses them in soft tissue image contrast for better visualization and tracking of soft tissue tumors with no additional radiation dose to the patient. A pre-clinical integrated 1.5 T magnetic resonance imaging and 7 MV linear accelerator system (MR-linac) allows for real-time tracking of soft tissues and adaptive treatment planning prior to each treatment fraction. However, due to the presence of a strong magnetic field from the MR component, there is a three dimensional (3D) change in dose deposited by the secondary electrons. Especially at nonhomogeneous anatomical sites with tissues of very different densities, dose enhancements and reductions can occur due to the Lorentz force influencing the trajectories of secondary electrons. These dose changes at tissue interfaces are called the electron return effect or ERE. This study investigated the ERE using 3D dosimeters.

1. Introduction

An integrated 1.5 T magnetic resonance imaging and 7 MV linear accelerator system (MR-linac, Elekta AB, Stockholm, Sweden) is under development as an image-guided radiation therapy system. Designed with the strong magnetic field (B-field) of the MR component perpendicular to the linac beam, the MR-linac allows for superior soft tissue image contrast compared to CT and MV or kV on-board imagers. However, the design of the MR-linac system presents some dosimetric concerns on secondary particle trajectories due to the Lorentz force. This is especially true for any interfaces with organs that contain air such as soft tissue-lung interfaces [1, 2]. Hot spots occur at transitions from high to low density structures, and cold spots occur at transitions from low to high density structures. These hot and cold spots are due to the Lorentz force directing the secondary electrons back into the higher density medium and is commonly called the electron return effect (ERE). The ERE has been simulated using various Monte Carlo codes, suggesting that the dose enhancement at water-air interfaces can be up to a factor of 1.6 and at soft tissue-lung interfaces up to a factor of 1.5 [1-4]. The ERE depends on several factors, such as machine-defined B-field strength and linac beam energy and patient anatomy-defined tissue interfaces and interface shapes. These factors result in a 3D change in dose distribution where sparse sampling of points using conventional point and 2D array dosimeters may no longer be sufficient to

demonstrate agreement with the treatment plan over the irradiated volume. For these reasons, 3D validation of dose delivery in the MR-linac may be necessary due to the various tissue interfaces within a human body, such as at the lung or trachea, that may result in out-of-plane dose perturbations.

As modern radiation therapy has become more complex with IMRT, VMAT, IGRT, and other treatment techniques, many forms of 3D dosimetry have been presented as tools for acquiring true volumetric dose distributions with continuous integrated dose measurements [5-9]. In this study, we utilized two types of 3D dosimeters to assess the acquisition of volumetric dose distributions in the MR-linac. Each dosimeter contained a cylindrical air cavity to induce the ERE.

2. Materials and Methods

The two types of dosimeters used for this study were radiochromic plastic PRESAGE® (Heuris Pharma, LLC, Skillman, NJ) and radiochromic gel FOX. PRESAGE® was first introduced in 2003 and has already been used for assessing IMRT and other complex treatment techniques [5-9]. The in-house made PRESAGE® dosimeters underwent an optically-visible change (clear to dark green color) upon irradiation due to the formation of malachite green from leuco malachite green (LMG). Each PRESAGE® dosimeter was prepared with a concentric cylindrical air cavity (1.5 cm diameter air cavity, 7.2 cm diameter dosimeter).

FOX was formulated in-house and had a Fricke-like composition but with greater MR contrast [10]. Similar to Fricke dosimeters, our FOX formulation underwent iron (II) oxidation upon absorbing radiation dose, resulting in optical (yellow to purple color) and MR-visible changes. Each FOX dosimeter was prepared in an 8.8 cm diameter petri dish, and a concentric cylindrical glass vial was initially inserted into the gel to mold a 2.5 cm diameter air cavity. The glass vial was removed before the gel was completely set to reduce disruption of the gel matrix.

The FOX dosimeter was primarily composed of water and was nearly equivalent to water and soft tissues (elemental compositions and effective atomic number (Z_{eff}) are listed below in Table 1). PRESAGE® had a greater Z_{eff} with its primarily polyurethane plastic composition [11].

Table 1. Elemental compositions of materials (weight fractions denoted as w_k) and Z_{eff}

Material	w_H	w_N	w_O	w_C	w_S	w_{Cl}	w_{Br}	w_{Fe}	w_{Na}	Z_{eff}
PRESAGE® [11]	0.0892	0.0446	0.2172	0.6074	-	0.0333	0.0083	-	-	8.65
FOX	0.1098	2.66E-6	0.8819	0.0081	1.12E-7	-	-	1.10E-4	1.56E-10	7.42
Water	0.1119	-	0.8881	-	-	-	-	-	-	7.42
Muscle	0.1042	0.0350	0.7289	0.1230	0.0050	-	-	-	-	7.46

2.1. Irradiation set-up with MR-linac

Both types of dosimeters were irradiated in the same set-up with the MR-linac. The direction of the B_0-field was along the axis of the cylindrical hole, which was centered within each cylindrical dosimeter. The linac beam (15 x 15 cm^2 field) entered perpendicularly to the B_0-field and cylindrical axis of the dosimeters (Figure 1).

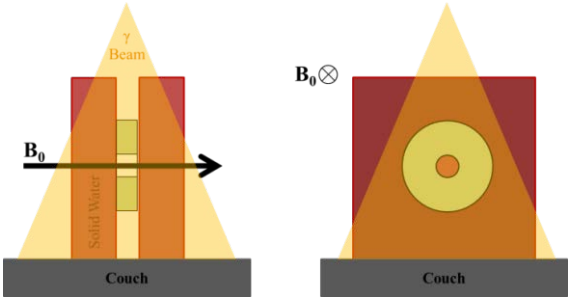

Figure 1. Irradiation set-up with MR-linac.

2.2. Dosimeter readout techniques

Two hours after irradiation, PRESAGE® dosimeters were readout using an optical-CT technique with the Duke Midsized Optical-CT System (DMOS) [12]. The dosimeter was placed on a rotating pedestal inside a refractive-index-matched fluid. Data were recorded for each angle at 1º intervals and reconstructed into a 3D data set.

FOX dosimeters were analyzed during and immediately after irradiation using the MR component of the MR-linac with balanced-Fast Field Echo (b-FFE) and T1-weighted sequences. Slices 5-mm thick were acquired for each dosimeter and combined into a 3D data set.

3. Results and Discussions

3.1. Experimental PRESAGE® results

Cross-sectional slices of the dose distributions for the PRESAGE® dosimeter showed a clear demonstration of the dose enhancement (red area) due to the ERE above the cavity (high to low density interface) and a region of reduced dose (blue area) below the cavity (low to high density interface) (Figure 2a).

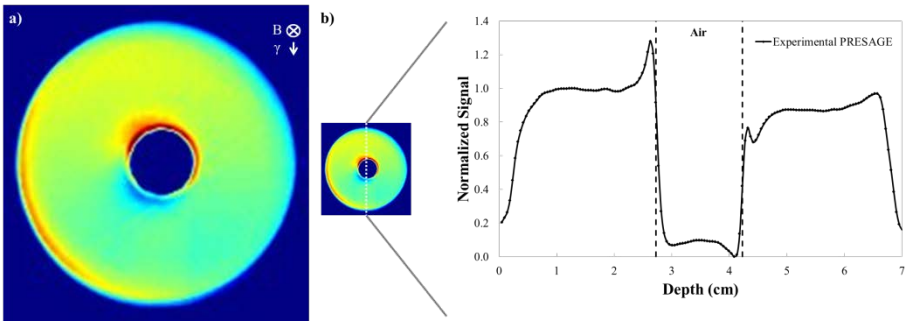

Figure 2. a) Cross-sectional slice of PRESAGE® and b) line profile.

The regions of increased and reduced doses were slightly rotated with respect to the radiation beam axis due to the average direction change of the electrons [2, 3]. Measurements from line profiles showed the dose enhanced to about 0.5 cm around the cavity for the PRESAGE® dosimeter by up to 30% (Figure 2b). The relative signal decreased 20% at cold spots for PRESAGE®.

3.2. Experimental FOX results

After irradiation, cross-sectional slices of the dose distributions for FOX dosimeters similarly showed a clear demonstration of the dose enhancement due to the ERE above the cavity and a region of reduced dose below the cavity (Figure 3a). Measurements from line profiles showed the dose enhanced to about 0.5 cm around the cavity by up to approximately 40% and reduced to about the same distance by 20% for FOX (Figure 3b).

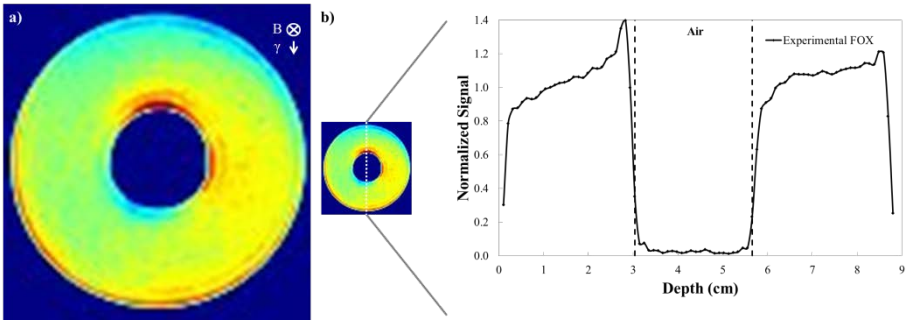

Figure 3. a) Cross-sectional slice of FOX and b) line profile.

Because the FOX dosimeter could be analyzed using MR measurements, near real-time cross-sectional slices were also acquired during irradiation. Snap shots of 6 dose points are shown in Figure 4a where the overall MR signal changes can be seen in the cross-sectional slices. However, the spatial resolution of these real-time images were not suitable for measuring the ERE in real-time (Figure 4b).

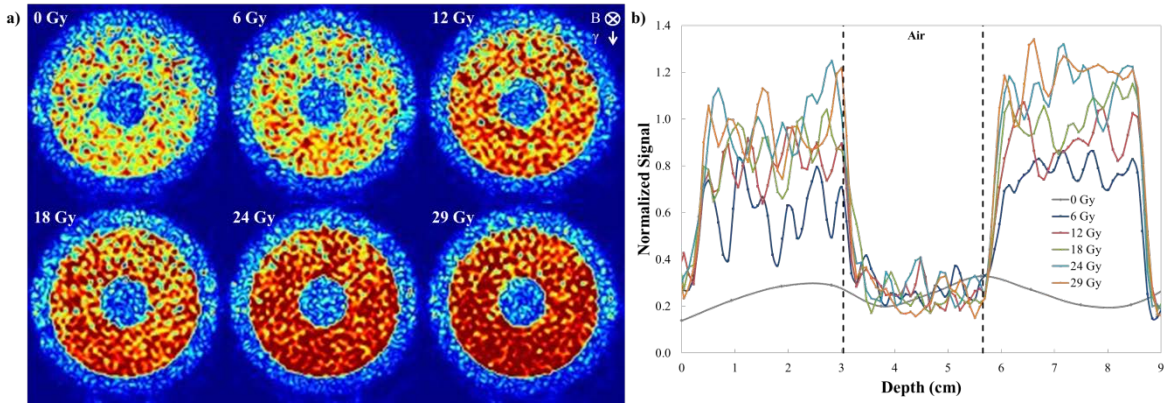

Figure 4. a) Cross-sectional slice snap shots of FOX during irradiation (approximate dose values to the center of the dosimeter) and b) line profiles.

4. Conclusions

The results of this study confirmed the feasibility of using radiochromic plastic PRESAGE® and radiochromic gel FOX for MR-linac and other MR-IGRT applications. Our results agreed well with Monte Carlo simulation results in the literature (assuming a water medium) with dose enhancement by up to 30-40% in a 1.5 T B-field for similar sized air cavities [2]. This study encourages the use of 3D dosimetry for rigorous QA of MR-IGRT in a volumetric acquisition and will be particularly advantageous at heterogeneous sites. The 3D dose readout for PRESAGE® has the advantage of greater spatial resolution with optical measurements whereas the FOX dosimeter has the advantage of readout in the same position as irradiation within the MR-linac using MR measurements, as well as the capability for real-time measurements.

5. References

[1] Lee H *et al* 2015 *Med. Phys*. **42** 3312
[2] Raaijmakers A J E *et al* 2005 *Phys. Med. Biol.* **50** 1363-76
[3] Raaijmakers A J E *et al* 2008 *Phys. Med. Biol.* **53** 909-23
[4] Rubinstein A E *et al* 2015 *Med. Phys.* **42** 5510-6
[5] Juang T *et al* 2013 *J. Phys.: Conf. Ser*. **444** 12080
[6] Lafratta R J *et al* 2015 *Phys. Conf. Ser*. **573** 012055
[7] Jackson J *et al* 2015 *Phys. Med. Biol.* **60** 2217–2230
[8] Schreiner L J 2015 *J. Phys.: Conf. Ser*. **573** 012003
[9] Baldock C *et al* 2010 *Phys. Med. Biol*. **55** R1-63
[10] Lee H *et al* 2016 *Med. Phys.* **43** 3660
[11] Brown S *et al* 2008 *Appl. Radiat. Isot.* **66** 1970-4
[12] Newton J *et al* 2010 *J. Phys.: Conf. Ser*. **250** 12078